Journal of Biomolecular NMR (2007) 37:159–177
DOI 10.1007/s10858-006-9091-0

Article

Unraveling protein dynamics through fast spectral density mapping

Virginie Ropars[a], Sabine Bouguet-Bonnet[b], Daniel Auguin[a], Philippe Barthe[a], Daniel Canet[b] & Christian Roumestand[a,*]

[a]*Centre de Biochimie Structurale, UMR UM1/5048 CNRS/554 INSERM, 29 rue de Navacelles, 34090 Montpellier Cedex, France;* [b]*Méthodologie RMN (UMR 7565 CNRS-UHP, Nancy 1), Université H. Poincaré, Nancy 1, BP 239, 54506 Vandoeuvre-lès-Nancy Cedex, France*

Received 7 July 2006; Accepted 22 September 2006

Key words: protein dynamics, ^{15}N relaxation, spectral density mapping

Abstract

Spectral density mapping at multiple NMR field strengths is probably the best method to describe the dynamical behavior of a protein in solution through the analysis of ^{15}N heteronuclear relaxation parameters. Nevertheless, such analyses are scarcely reported in the literature, probably because this method is excessively demanding in spectrometer measuring time. Indeed, when using n different magnetic fields and assuming the validity of the high frequency approximation, the discrete sampling of the spectral density function with $2n + 1$ points needs the measurement of $3n$ ^{15}N heteronuclear relaxation measurements (nR_1, nR_2, and n^{15}N{^{1}H}NOEs). Based on further approximations, we proposed a new strategy that allows us to describe the spectral density with $n + 2$ points, with the measurement of a total of $n + 2$ heteronuclear relaxation parameters. Applied to the dynamics analysis of the protein p13^{MTCP1} at three different NMR fields, this approach allowed us to divide by nearly a factor of two the total measuring time, without altering further results obtained by the "model free" analysis of the resulting spectral densities. Furthermore, simulations have shown that this strategy remains applicable to any low isotropically tumbling protein (τ_c>3 ns), and is valid for the types of motion generally envisaged for proteins.

Abbreviations: ^{15}N{^{1}H}NOE – heteronuclear ^{15}N nuclear Overhauser enhancement; $R_N(N_z)$ (R_1) – heteronuclear ^{15}N longitudinalrelaxation rate; $R_N(N_{xy})$ (R_2) – heteronuclear ^{15}N transverserelaxation rate; $R_N(H_z -> N_z)$ (σ) – cross-relaxation rate between^{15}N and its attached amide proton.

During the past 30 years, both experimental and theoretical studies of proteins have provided a wealth of data about their internal dynamics that have severely hustle the conventional view of a protein structure as a static arrangement of atoms in space (Austin et al., 1975; Wagner and Wüthrich, 1978; Mulder et al., 2001; Palmer 2004; Atkinson and Kieffer, 2004; Eisenmesser et al., 2005). A particularly powerful approach has been NMR spectroscopy that has revealed that proteins are highly flexible, and, more importantly, that their intrinsic dynamics can be linked to their function in several ways. In the last decade, such studies have been preferentially dealt with by means of ^{15}N relaxation rate measurements in isotopically enriched protein samples, thereby allowing the local dynamics along the protein backbone to be explored.

The dynamical information content of the ^{15}N heteronuclear relaxation rate constants consists of discrete evaluation of the spectral density

*To whom correspondence should be addressed. E-mail: christian.roumestand@cbs.cnrs.fr

functions corresponding to the various ^{15}N–^{1}H bonds of the protein. The spectral densities are typically denoted by $J(\omega)$ and reflect the power spectra pertaining to the orientational fluctuations of ^{15}N–^{1}H bonds relative to the external field B_0. Peng and Wagner have proposed a strategy in which one measures a set of six relaxation parameters for the ^{15}N–^{1}H bonds at a given B_0 field strength (Peng and Wagner, 1992a, b). Such measurements provide directly the spectral density values from experimental data and thereby map the spectral density functions for each ^{15}N–^{1}H bond. Contrary to approaches where models are used to interpret the NMR relaxation data, the reliability of the dynamical information in the spectral density mapping approach depends *only* upon the accuracy of the NMR experiments, not upon the inherent assumptions of the model. Nevertheless, random as well as systematic errors for some of the measured relaxation rates make it difficult to determine $J(\omega)$ at high frequencies, namely $J(\omega_H)$ and $J(\omega_H \pm \omega_N)$ where ω_H and ω_N represent the proton and nitrogen resonance frequencies (in rad/s), respectively. Assuming a slow variation of $J(\omega_H)$ around the proton frequency for low tumbling proteins alleviates this difficulty. This so-called ''high frequency approximation'' (Peng and Wagner, 1992a, 1992b; Farrow et al., 1995; Ishima and Nagayama, 1995a, b; Lefèvre et al., 1996) leads to the ''reduced spectral density mapping'' through the determination of $J(0)$, $J(\omega_N)$ and $\langle J(\omega_H)\rangle$ (the ''average'' value of $J(\omega)$ for $\omega_H - \omega_N$, ω_H and $\omega_H + \omega_N$ frequencies), with the measurement of only three heteronuclear relaxation rates, usually the longitudinal relaxation rate (R_1), the transverse relaxation rate (R_2) and the ^{1}H–^{15}N cross-relaxation rate σ_{NH}, the latter being deduced from the measurement of the heteronuclear $^{15}N\{^{1}H\}$NOE (Nuclear Overhauser Effect). Such a combination of relaxation rates has the advantage of not employing proton relaxation which involves dipolar interactions with other protons thus making its interpretation more difficult. As a matter of fact, this approach entails a considerable experimental time saving, since it requires only three relaxation rates. The drawback of this method resides in a poor description of the spectral density function since only three points are available for describing the whole curve and this can prove notably insufficient for the description of complex motions. A straightforward way to obtain a better description of the shape of density function is to measure ^{15}N relaxation rates at multiple NMR fields (Peng and Wagner, 1995; Vis et al. 1998; Canet et al., 2001; Bouguet-Bonnet et al., 2005a, b): recording data at n field strengths will provide $2n + 1$ discrete values of the spectral density function (i.e., $J(\omega_N)$ and $\langle J(\omega_H)\rangle$ for each value of the B_0 field strength and $J(0)$), but at the expense of a very long measuring time since $3n$ relaxation experiments must be performed (nR_1, nR_2 and $n^{15}N\{^{1}H\}$NOE experiments). Here, we propose an alternative method based on an additional approximation that takes into account the very different relative contributions of the spectral densities at 0, ω_N, and $<\omega_H>$ frequencies to the longitudinal and transverse relaxation rates, and to the ^{1}H–^{15}N cross-relaxation rate in the case of low tumbling proteins. As long as this approximation is valid, $n + 2$ discrete values of the spectral density function are deduced from $n + 2$ relaxation experiments which are the measurements of the transverse relaxation rate R_2 and the heteronuclear $^{15}N\{^{1}H\}$NOE experiment at a given field strength, in addition to R_1 relaxation rates for each field strength. We show in the following through simulations and by means of a practical example that this method provides as accurate results as the conventional ''reduced spectral density mapping''. Owing to the considerable experimental time saving, we called this approach ''fast spectral density mapping''.

Material and methods

Theoretical background for simulations

When the relaxation of the ^{15}N nucleus is predominantly caused by the dipolar interaction with its attached amide proton and by the anisotropy of its chemical shift, the longitudinal relaxation rate $R_N(N_z)$, the transversal relaxation rate $R_N(N_{xy})$ and the ^{1}H–^{15}N cross-relaxation rate (denoted R_1, R_2 and σ_{NH} in the following, respectively) depend on the spectral density function at five different frequencies (Abragam, 1961):

$$R_1 = (3D + C)J(\omega_N) + DJ(\omega_H - \omega_N) + 6DJ(\omega_H + \omega_N) \quad (1)$$

$$R_2 = \left(2D + \frac{2C}{3}\right) J(0) + \left(\frac{3D}{2} + \frac{C}{2}\right) J(\omega_N) + \frac{D}{2} J(\omega_H - \omega_N) + 3DJ(\omega_H) + 3DJ(\omega_H + \omega_N) + R_{ex} \quad (2)$$

$$\sigma_{NH} = D[6J(\omega_H + \omega_N) - J(\omega_H - \omega_N)] \quad (3)$$

in which $D = (\frac{\mu_0}{4})^2 \frac{h^2 \gamma_X^2 \gamma_H^2}{4\pi^2 r_{XH}^6}$ and $C = \frac{1}{3}(\gamma_N B_0)^2 \Delta\sigma^2$ where μ_0 is the permeability of vacuum, h is Planck's constant, γ_H (2.6752×10^8 rad s^{-1} T^{-1}) and γ_N (-2.711×10^7 rad s^{-1} T^{-1}) are the gyromagnetic ratios of the ^1H and the ^{15}N nuclei, respectively, and ω_H and ω_N are the ^1H and ^{15}N Larmor frequency, respectively; r_{NH} is the internuclear ^1H–^{15}N distance (1.02 Å), B_0 is the magnetic field strength, and $\Delta\sigma$ is the difference between the parallel and perpendicular components of the axially symmetric ^{15}N chemical shift tensor, estimated to be −170 ppm (Tjandra et al., 1996; Lienin et al., 1998; Fushman et al., 1999) for all residues: this point will be discussed further; R_{ex} is the exchange contribution to the transverse relaxation rate, that will be neglected in the following simulations.

Assuming that ^1H–^{15}N vectors are subjected to more or less complex combinations of diffusive motions, and limiting our investigation to isotropically tumbling proteins, we used the following models of spectral density functions for our simulations:

$$J(\omega) = \frac{2}{5}\left\{\frac{\tau_c}{1 + (\omega\tau_c)^2}\right\} \quad (4)$$

$$J(\omega) = \frac{2}{5}\left\{S^2 \frac{\tau_c}{1 + (\omega\tau_c)^2} + (1 - S^2)\frac{\tau}{1 + (\omega\tau)^2}\right\} \quad (5)$$

$$J(\omega) = \frac{2}{5}\left\{S_f^2 S_s^2 \frac{\tau_c}{1 + (\omega\tau_c)^2} + S_f^2(1 - S_s^2) \frac{\tau}{1 + (\omega\tau)^2} + (1 - S_f^2)\frac{\tau'}{1 + (\omega\tau')^2}\right\}. \quad (6)$$

The single Lorentzian function reported in Equation (4) corresponds to the "rigid-body" model, the protein behaving as a rigid sphere, and the ^1H–^{15}N vectors sensing only the protein tumbling time τ_c. This very simple motion is scarcely encountered in proteins, hence the use of more complicated motion models used to fit the relaxation times: generally a sum of Lorentzian functions, as the ones proposed in Equations (5) and (6). Equation (5) corresponds to the well-known Lipari–Szabo "Model Free" (Lipari and Szabo, 1982) approach for which overall and internal motions are assumed to contribute independently to the reorientational time correlation function of the ^1H–^{15}N vectors, internal motions being also supposed to occur on a much faster time scale than the global rotation of the molecule. According to this approach, τ is deduced from the overall motion correlation time τ_c and the internal motion correlation time τ_f pertaining to each residue: $\tau^{-1} = \tau_c^{-1} + \tau_f^{-1}$ (very often $\tau \cong \tau_f$). The square of a generalized order parameter S^2, ranging from 0 to 1, characterizes the restriction of internal motions. In some cases, the simple form of Equation (5) turns out to be insufficient to fit the whole set of experimental data. This occurs when residues exhibit internal motions in a time window close to 1 ns. In this case, the expression for the spectral density function is extended to the one given in Equation (6) (Clore et al., 1990a, b). In this "Extended Lipari–Szabo" model, $\tau^{-1} = \tau_c^{-1} + \tau_s^{-1}$ and $\tau^{-1} = \tau_c^{-1} + \tau^{-1} \cdot S_f^2$ and S_s^2 and the square of the partial order parameters for fast (τ_f, picosecond time scale) and slow (τ_s, sub-nanosecond time scale) internal motions, respectively. The square of the generalized order parameter S^2, defined as $S_f^2 S_s^2$, is a measure of the total amplitude of the internal motions. Assuming that the contribution of the fastest motion to the spectral density function is negligible, the spectral density function can be written as follow :

$$J(\omega) = \frac{2}{5}\left\{S_f^2 S_s^2 \frac{\tau_c}{1 + (\omega\tau_c)^2} + S_f^2(1 - S_s^2)\frac{\tau}{1 + (\omega\tau)^2}\right\} \quad (7)$$

Equation (7) was used for the simulation of two kinds of different motion frequently encountered

in proteins: completely disordered motions, often encountered in the terminal residues of a protein, and hinge motions that correspond to collective motions of a given number of residues in the protein. Contrary to disordered motions, characterized by a concomitant decrease of both S_f^2 and S_s^2, hinge motions are generally sub-nanosecond motions (described by τ_s and S_s^2) that can affect structured segments of the protein, such as helices or sheets, associated with restricted internal motions (S_f^2 close to 1) (for an example: Barthe et al., 1999).

Equations (4), (5) and (7) were used to calculate spectral densities that were inserted in turn into Equations (1) to (3) to calculate relaxation times at five magnetic field strength ranging from 9.4 to 18.8 T (corresponding to proton frequencies of 400, 500, 600, 700 and 800 MHz). The value of τ_c was varied between 3 and 30 ns: the lowest value corresponds more or less to the validity limit of the high frequency approximation that will be used further in the simulations, whereas the highest value corresponds to the limit of the protein size (about 300 residues) above which conventional NMR relaxation measurements are hardly feasible. To simplify, simulations using Equation (7) were restricted to protein tumbling time τ_c of 3, 10, and 30 ns, with the value of S_f^2 fixed to 0.8 in case of hinge motion (S_s^2 scaling from 0.1 to 0.9), or varying between 0.1 and 0.9, concomitantly with S_s^2, in case of disordered motions.

Then, with the help of the equations given below, the simulated relaxation times were used to recalculate $J(0)$, $J(\omega_N)$ and $\langle J(\omega_H)\rangle$ as if relaxation rates were experimentally determined.

$$J(0) = \frac{3}{2}\frac{1}{3D + C}\left(R_2 - \frac{1}{2}R_1 - \frac{3}{5}\frac{\gamma_N}{\gamma_H} \times \mathrm{NOE} \times R_1\right) \quad (8)$$

$$J(\omega_N) = \frac{1}{3D + C}\left(R_1 - \frac{7}{5}\frac{\gamma_N}{\gamma_H} \times \mathrm{NOE} \times R_1\right) \quad (9)$$

$$\langle J(\omega_H)\rangle = \frac{1}{5D}\frac{\gamma_N}{\gamma_H} \times \mathrm{NOE} \times R_1 \quad (10)$$

Note that, to be consistent with the experimental procedures, σ_{NH} has been substituted for the quantity denoted as NOE (equal to I/I_0-1, where I and I_0 are the ^{15}N signal amplitudes with and without irradiation at the proton resonance frequency). σ_{NH} is related to NOE by the following relation: $\mathrm{NOE} = (\gamma_H/\gamma_N)\cdot\sigma_{NH}/R_1$. These equations take in account the high frequency approximation: $\langle J(\omega_H)\rangle$ represents the "average" value of $J(\omega)$ at $\omega_H - \omega_N$, ω_H and $\omega_H + \omega_N$ frequencies. In the multifield spectral density mapping approach, spectral densities are calculated from the relaxation rates R_1, R_2 and the NOE obtained at each magnetic field value, whereas a combination of relaxation rates obtained at different magnetic field strengths will be used for the fast spectral density mapping, as it will be detailed in the "Results and discussion" section.

Experimental

Uniformly enriched ^{15}N p13^{MTCP1} was obtained as previously reported (Yang et al., 1998; Guignard et al., 2000). NMR experiments were carried out at 9.4, 11.75 and 14.1 T on Bruker Avance 400, 500 and 600 spectrometers equipped with 5 mm *z*-gradient ^1H–^{13}C–^{15}N triple resonance probes. Protein sample (1 mM) was dissolved in a 10 mM Tris–HCl buffer, pH 7.0, with 5% ^2H_2O for field-frequency stabilization. The temperature was carefully adjusted using a calibration sample (80% glycol in d_6-DMSO) and set at 20 °C. In all experiments, the ^1H carrier was centred on the water resonance and a WATERGATE (Piotto et al., 1992; Sklenar, 1995) sequence was incorporated to suppress the solvent resonance. Quadrature detection in the indirect dimensions was achieved using States-TPPI (Marion et al., 1989). The pulse sequences for determining ^{15}N R_1, R_2, and $^{15}N\{^1H\}$NOE values are those classically used (Peng and Wagner, 1992a, b; Kay et al., 1992), while experimental parameters and processing as previously reported (Guignard et al., 2000). Briefly, a recycle delay of 4 s was employed in R_1 and R_2 experiments, and ^{15}N decoupling during acquisition was performed using a WALTZ sequence. R_1 experiments were performed with nine relaxation delays T (18, 30, 78, 162, 222, 438, 942, and 1206 ms). R_2 experiments were carried out employing a Carr–Purcell–Meiboom–Gill (CPMG) pulse train (Carr and Purcell, 1954;

Meiboom and Gill, 1958) with nine relaxation delays T of 8, 16, 32, 48, 64, 80, 96, 112, and 128 ms. The 90° ^{15}N pulse width was adjusted at 50 μs for all B_0 field values. All experiments were recorded with a time domain data size of 128 t_1 × 1K t_2 complex points and eight transients (16 at 400 MHz) per complex t_1 increment, yielding a total measuring time of about 12 h (24 h at 400 MHz) for each series of experiments. In heteronuclear ^{15}N{^{1}H}NOEs, proton saturation was achieved during the relaxation time by application of high-power 120° pulse spaced at 20 ms intervals for 3 s prior to the first pulse on ^{15}N (Kay et al., 1989). A relaxation delay equal to 6 s between each scan was used in order to obtain a complete relaxation of water magnetization and to reduce effects arising from amide proton exchange. The two experiments – with and without proton saturation – were acquired in an interleaved manner, FID by FID, with the same time domain data size as for the R_1 and the R_2 experiments, and 32 transients (64 at 400 MHz) per complex t_1 increment, yielding a total measuring time of about 15 h (30 h at 400 MHz).

Results and discussion

Simulations

When proceeding according to the spectral density mapping approach to analyze relaxation data recorded at nB_0 field values, the measurement of a complete set of relaxation parameters (R_1, R_2 and NOE) for each magnetic field value is required, yielding n values of $J(\omega_N)$, n values of $\langle J(\omega)\rangle$, and only one value of $J(0)$. If one disregards the possible contribution of exchange contributions (this will be discussed later), it appears that the information on $J(0)$ is highly redundant, since this spectral density value should be evidently independent of the magnetic field value. Hence, the information on this particular quantity can be readily obtained through the measurement of the ^{15}N heteronuclear relaxation parameters at a single NMR field value. Moreover, if we limit ourselves to the case of low tumbling proteins, where R_1, R_2 and σ_{NH} currently differ from each others by about an order of magnitude, Equation (8) shows that $J(0)$ is largely determined from R_2 values, with however a non-negligible contribution of R_1 values when $\omega\tau_c$ decreases, while the contribution of σ is not decisive. As a result, while the measurement of R_2 and R_1 needs to be done at the same B_0 field, the NOE value used in Equation (8) can be obtained at a different B_0 without altering significantly the resulting value of $J(0)$. This has been checked through simulations (see "Materials and methods" section), comparing $J(0)$ values calculated through Equation (8) with R_1 and R_2 obtained at 9.4 T, and NOE values obtained either at 9.4 or 18.8 T. For τ_c values ranging from 3 to 30 ns, virtually identical values are obtained whatever the model of motion (Figure 1).

Furthermore, if one assumes that a good description of the lorentzian function around $J(\omega_N)$ is able to discriminate between the different kinds of motions – as we demonstrate further through simulations and experimental verifications – one point at high frequency on the $J(\omega)$ curve will be sufficient to characterize it. As a result, a single couple of NOE and R_1 values can provide the value of $\langle J(\omega_H)\rangle$. Contrary to $J(0)$, and because the value of $\langle J(\omega_H)\rangle$ depends (and depends *only*) on the product NOE × R_1 (see Equation (10)), these two relaxation parameters *must* be measured at the same B_0 field: thus, the value obtained for $\langle J(\omega_H)\rangle$ corresponds to its *exact* value, within the high frequency approximation limits. Subsequently, an extensive sampling of the spectral density around $J(\omega_N)$ can be derived through the measurement of R_1 rates *only*, at each B_0 magnetic field. Indeed, Equation (9) shows that the $J(\omega_N)$ value is essentially dominated by R_1, with – in the case of low tumbling molecules – only a weak contribution of σ_{NH} which can therefore be approximated by the one already used for the calculation of $\langle J(\omega_H)\rangle$. As a result, the exact value of $J(\omega_N)$ is obtained only for the magnetic field strength at which both R_1 and NOE are measured ($J(80)$ in our simulations). Simulations performed as described above show only a weak deviation from the exact value for the other magnetic induction values (Figures 2–5): whatever the model of motion, this deviation becomes apparent for the lowest value of $J(\omega)$ ($J(40)$) calculated with the lowest tumbling times ($\tau_c < 5$ ns). When using the Lipari–Szabo approach, deviations from the exact value of $J(40)$ slightly increase with the value of the order parameter S^2 (Figure 3). A similar variation is observed with the extended Lipari–Szabo approach in case of hinge motion

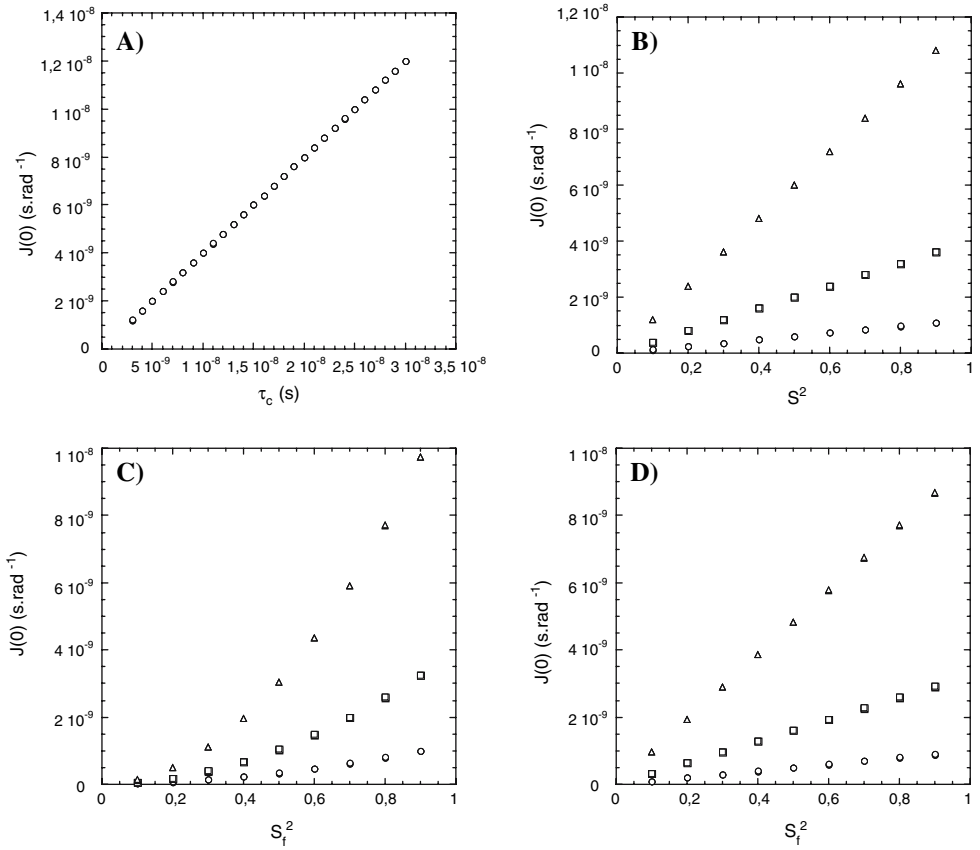

Figure 1. Comparison of $J(0)$ values obtained through Equation (8) with either the regular spectral density mapping (open symbols; ^{15}N R_1, R_2 and ^{15}N{^{1}H}NOE calculated for a B_0 field of 9.4 T) or the fast spectral density mapping approach (filled symbols; ^{15}N R_1 and R_2 calculated for a B_0 field of 9.4 T, ^{15}N{^{1}H}NOE calculated for a B_0 field of 18.8 T). Relaxation rates used in Equation (8) were calculated using Equations (1) to (3), where spectral densities have been simulated for different kind of protein dynamics behavior through: Equation (4), for "rigid-body" motions (3 ns $< \tau_c <$ 30 ns) (A); Equation (5), for motions compatible with the Lipari–Szabo formalism ($0 < S^2 < 1$) (B); Equation (7) for disordered random motion (Extended Lipari–Szabo formalism with $0 < S_f^2 = S_s^2 < 1$) (C) or hinge motions (Extended Lipari–Szabo formalism with $S_f^2 = 0.8$ and $0 < S_s^2 < 1$ (D). For the sake of clarity, when the Lipari–Szabo formalisms ("simple" or extended) were used, the corresponding spectral densities were only calculated for τ_c values equal to 3 ns (circles), 10 ns (squares), and 30 ns (triangles). In this figure and in the following, filled symbols are in the background.

($S_f^2 = 0.8$, $0.1 < S_s^2 < 0.9$) (Figure 5), whereas disordered random motions ($0.1 < S_s^2 = S_f^2 < 0.9$) show a different behavior, depending on the τ_c value: for low τ_c values, deviations increase with the value of the order parameter S^2, whereas the reverse is observed for high τ_c values (30 ns). In that latter case, deviations are rather weak (Figure 4).

The next step was to evaluate the incidence of these small deviations on the results of the analysis of the spectral densities through different models of motion. To this aim, we calculated different sets of $J(\omega)$ values at 0, 40, 50, 60, 70, 80, 400, 500, 600, 700, and 800 MHz through Equations (8) to (10), using either the conventional or the fast spectral density mapping approach. The ^{15}N R_1, R_2, and NOE relaxation parameters used in these equations were calculated from Equations (1) to (3) for three different types of motions: the simplest one corresponds to a spectral density function that has been modeled with the simple Lipari–Szabo expressions (Equation (5)), whereas random disordered motions and hinge motion were modeled according to the Extended Lipari–Szabo expressions (Equation (7)), as described in the "Material and Methods" section. In order to keep our analysis in reasonable limits, we restrict the simulations to three τ_c values: 3, 10, and 30 ns. As a result, we obtained nine

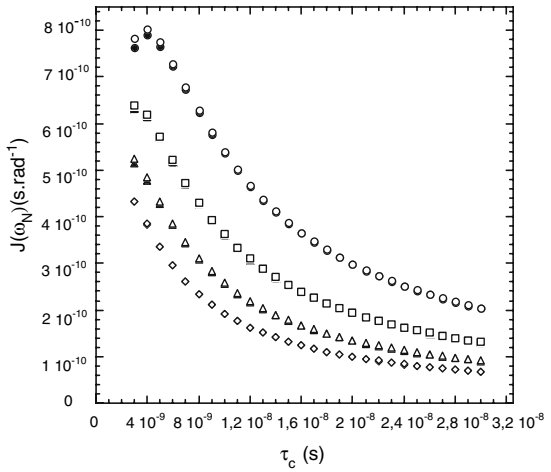

Figure 2. Comparison of $J(\omega_N)$ values obtained through Equation (9) with either the regular spectral density mapping (open symbols; $^{15}NR_1$ and $^{15}N\{^1H\}NOE$ calculated for each value of the B_0 field) or the fast spectral density mapping approach (filled symbols; $^{15}NR_1$ calculated for each B_0 induction, $^{15}N\{^1H\}NOE$ calculated *only* for a B_0 field of 18.8 T). Circles, squares, triangles and diamonds stands for $J(40)$, $J(50)$, $J(60)$ and $J(70)$, the two approaches give the same value for $J(80)$. The values between parentheses referred to the ^{15}N resonance frequency expressed in MHz: 40, 50, 60, 70, 80 for B_0 = 9.4, 11.7, 14.1, 16.5, 18.8 T, respectively. Relaxation rates used in Equation (9) were calculated using Equations (1) to (3), where spectral densities have been simulated for "rigid-body" motions (3 ns $< \tau_c <$ 30 ns) (Equation (4)).

different sets of $J(\omega)$ values for each approach, corresponding to three different models of motion, simulated with three different τ_c values. Each individual set of $J(\omega)$ values was then fitted with either the Lipari–Szabo or the Extended Lipari–Szabo models with our in-house written program DYNAMOF (www.cbs.cnrs.fr) (Barthe et al., 2006). In the SIMPLEX optimization process, only the τ_c value was fixed, and the S^2, S_s^2, S_f^2, τ_s and τ_f values were tentatively optimized starting from identical guess values whatever the model used. As a first result, the χ^2 analysis (data not shown) allows us to select the right model in any cases and for the two approaches, except for hinge motions and disordered motions with the highest value of generalized order parameter ($S^2 (= S_s^2 \times S_f^2) = 0.81$ for disordered motions, $S^2 = 0.72$ for hinge motions) where the simple Lipari–Szabo expression gives a better fit. The results of the different fits gathered in Tables 1–3 show that the order parameters (generalized or partial) are correctly retrieved by the two approaches with virtually identical values. As usually observed, the situation is not so good regarding correlation times whatever the strategy used. This stems from the high frequency approximation since τ_f is essentially deduced from $\langle J(\omega) \rangle$. The uncertainties on the corresponding values obtained through the fast spectral density mapping are generally higher than the ones obtained with the conventional spectral density mapping, probably due to the poorer sampling of the spectral density at high frequency.

Experimental

We have checked the validity of our simulations by comparing the experimental results obtained using either the conventional or the fast spectral density mapping approach applied to the analysis of the intrinsic dynamics of $p13^{MTCP1}$, a 13 kDa extensively studied oncogenic protein, the NMR structure of which has been solved in the laboratory (Yang et al., 1998; Guignard et al., 2000). The main structural motif of $p13^{MTCP1}$ is an orthogonal ß-barrel consisting of eight antiparallel ß strands of variable length, with a unique and common topology of this oncoprotein family (see Figure 8). The ß-strands are arranged into two very similar up-and-down four stranded ß-meander motifs, consisting of one short and one long two-stranded ß-sheet, which together form an L-shape. The ends of the long ß-strand pairs are not involved in the barrel hydrogen bond pattern, but protrude from the core of the molecule, forming two ß-pleated loops. The two ß-sheet motifs are connected by a long poorly structured loop (segment Gln48-Pro66), presenting a short helical segment (Arg56-Ser63). As demonstrated in a previous ^{15}N relaxation study, these different elements of structure exhibit very different dynamics behavior, hence the incitement to use this protein as a model for testing our approach.

^{15}N R_2, R_1 and $^5N\{^1H\}NOEs$ experimental values were obtained for 91 non-overlapping residues (at any frequency) among the 100 non-proline residues of the protein $p13^{MTCP1}$ from spectra recorded at 400, 500 and 600 MHz (Figure 6). Spectral density values at 0, 40, 50, 60, 348, 435 and 522 MHz were calculated from Equations (8) to (10) using either the conventional (reduced) spectral density mapping or the fast spectral density mapping (Figure 7A). For the latter, the

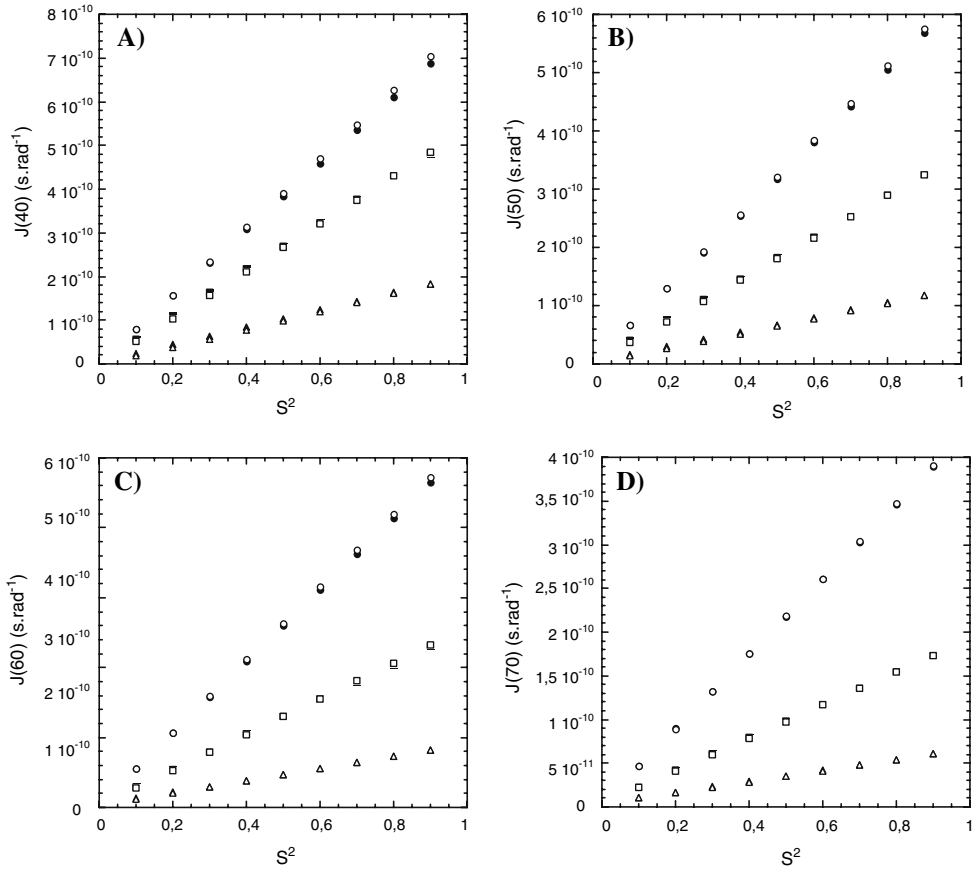

Figure 3. Comparison of $J(\omega_N)$ values obtained through Equation (9) with either the regular spectral density mapping (open symbols; ^{15}N R_1 and $^{15}N\{^1H\}$NOE calculated for each B_0 induction) or the fast spectral density mapping approach (filled symbols; ^{15}N R_1 calculated for each value of the B_0 field, $^{15}N\{^1H\}$NOE calculated *only* for a B_0 field of 18.8 T): (A) $J(40)$; (B) $J(50)$; (C) $J(60)$; (D) $J(70)$, the two approaches give the same value for $J(80)$. See Figure 2 for the meaning of numbers between parentheses. Relaxation rates used in Equation (9) were calculated using Equations (1)–(3), where spectral densities were in turn simulated for motions modelisable with the Lipari–Szabo formalism ($0 < S^2 < 1$) (Equation (5)). For the seak of clarity, only spectral densities corresponding to motions with global correlation times τ_c of 3 ns (circles), 10 ns (squares), and 30 ns (triangles) are reported.

$\langle J(522)\rangle$ values were calculated from R_1 and heteronuclear NOE measured at 600 MHz, and $J(0)$ values from R_2 rates measured at 400 MHz, as discussed above. The comparison of the two sets of $J(0)$ and $J(\omega_N)$ obtained with the two methods is presented on Figure 7B: as expected from our previous simulations, virtually identical values are obtained within the uncertainty range. This means that the two methods give a similar description of the spectral density function that can be tentatively used for describing qualitatively the intrinsic dynamics of the protein. Briefly, the low $J(0)$ values for the terminal residues as well as, though to a lesser extent, for the peptidic segments Glu35-Leu40 and Gln48-Leu65 are indicative of an increased flexibility. The segment Glu35-Leu40 is solvent-exposed and forms one of the structured ß-pleated loops which protrudes out of the ß-barrel. The segment Gln48-Leu65 forms the long poorly structured loop which joins the two ß-meanders, comprising the helical region. In these regions, smaller values of $J(0)$ for flexible residues with respect to the rigid part of the protein (the ß-barrel) are compensated for by high values of $\langle J(\omega_H)\rangle$. Low $\langle J(\omega_H)\rangle$ values for the rest of the protein indicate restricted flexibility on fast timescales. At 40 MHz, $J(\omega)$ values exhibit a trend similar to that observed for $J(0)$: a decrease is observed for NH vectors located on the loop and, to a lesser extent, for NH vectors located on the

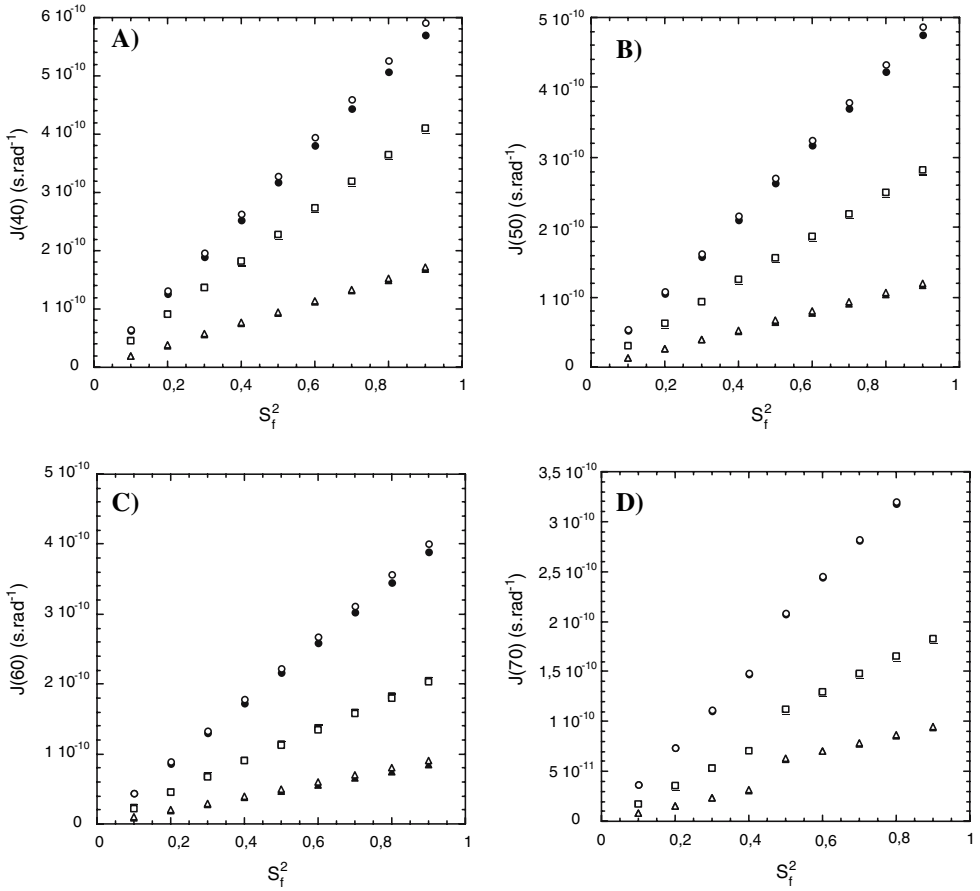

Figure 4. Same as Figure 3, except that the spectral densities used for the calculation of relaxation rates have been simulated for disordered random motion (Extended Lipari–Szabo formalism with $0 < S_f^2 = S_s^2 < 1$) (Equation (7)). For the sake of clarity, only spectral densities corresponding to motions with global correlation times τ_c of 3 ns (circles), 10 ns (squares), and 30 ns (triangles) are reported.

segment Glu35-Leu40. At 60 MHz, the distribution of $J(\omega)$ as a function of the residue number is almost flat, indicating proximity to the isobestic frequency, where the contribution of $J(\omega)$ is independent of the internal mobility. Some residues exhibit anomalous high values of $J(0)$ that are not compensated for by low values of $\langle J(\omega_H)\rangle$: this is indicative of exchange contributions in the μs to ms time-scale and this point will be discussed in more details later.

Again, the program DYNAMOF was used to extract the Lipari–Szabo parameters from the analysis of the spectral density functions calculated for the protein p13^{MTCP1}. The ratio of the principal components of the average inertia tensor for the backbone atom on the average structure of p13^{MTCP1} was determined to be (1.9:1.7:1.2). These numbers suggest that the overall rotation of the protein is expected to have only a small degree of anisotropy that may not have a significant influence, at least on the order parameters values (Tjandra et al., 1995). The global value of the overall rotational correlation time τ_c was taken as the average of the values obtained independently for those residues which were correctly (low χ^2) accommodated by the "simple" Lipari–Szabo formalism (Equation (5)) and showed order parameters higher than 0.70. This procedure led to a correlation time equal to 10.35 ± 0.37 ns or 10.26 ± 0.32 ns when using the conventional or the fast spectral density mapping strategy, respectively. Once the overall tumbling time τ_c has

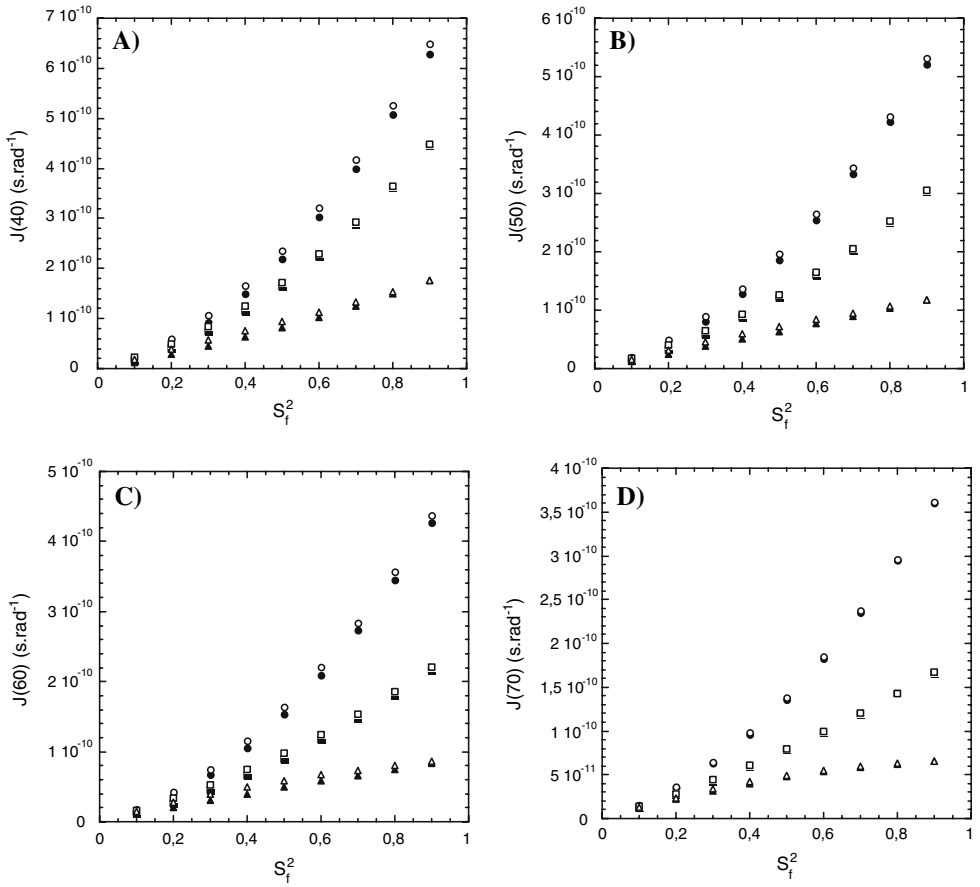

Figure 5. Same as Figures 3 and 4, except that the spectral densities used for the calculation of relaxation rates have been simulated for hinge motions (Extended Lipari–Szabo formalism with $S_f^2 = 0.8$ and $0 < S_s^2 < 1$ (Equation (7)). For the sake of clarity, only spectral densities corresponding to motions with global correlation times τ_c of 3 ns (circles), 10 ns (squares), and 30 ns (triangles) are reported.

been determined, model-free parameters were obtained by using either the ''simple'' or the ''extended'' (Equation (7)) Lipari–Szabo formalisms. We tentatively use the ''non-simplified extended'' Lipari–Szabo model (Equation (6)), introducing τ_f as fourth additional parameter for the fit, but this procedure did not give significant improvements. On the other hand, an additional fit was performed with the equation below in order to take an account possible exchange contributions to $J(0)$:

$$J(0)_{\text{obs}} = J(0)_{\text{cor}} + \lambda \cdot \phi \cdot \omega_N^2 \qquad (11)$$

where ϕ is the exchange factor ($R_{\text{ex}} = \phi \cdot \omega_N^2$) and λ a scaling factor ($\lambda = (3/2)[1/(3D + C)]$). $J(0)_{\text{obs}}$ stands for the $J(0)$ value calculated from the measured relaxation parameters, $J(0)_{\text{cor}}$ for the ''true'' value of $J(0)$, corrected from exchange contributions (Peng and Wagner, 1995).

As a first result and in agreement with the above simulations, whatever is the amide group in the protein sequence, the more appropriate formalism (Lipari–Szabo or the extended form) for fitting its associated spectral density function happened to be the same within the two approaches, as supported by a χ^2 analysis (not shown). The internal dynamics of most backbone NH vectors located in the ß-barrel are satisfactorily accounted for using Equation (5). For the N- and C-terminal residues, the use of Equation

Table 1. Motion parameters obtained by fitting simulated spectral densities obtained either with the conventional spectral density mapping or with the fast spectral density mapping (into brackets) in the case of the Lipari–Szabo model (τ_c was fixed at the value used in the simulations)

Lipari–Szabo Model						
τ_c (ns)	S^2			τ_f (ps)		
30	**0.1**	0.1 ± 0.01	(0.09 ± 0.01)	**10**	10.0 ± 0.45	(10.1 ± 1.1)
	0.2	0.2 ± 0.01	(0.19 ± 0.01)	**10**	9.7 ± 0.4	(9.7 ± 0.8)
	0.3	0.3 ± 0.01	(0.29 ± 0.01)	**10**	9.4 ± 0.5	(9.6 ± 1.1)
	0.4	0.4 ± 0.01	(0.39 ± 0.01)	**10**	9.2 ± 0.52	(9.5 ± 1.0)
	0.5	0.5 ± 0.01	(0.49 ± 0.01)	**10**	8.8 ± 0.49	(9.1 ± 1.1)
	0.6	0.6 ± 0.01	(0.60 ± 0.01)	**10**	8.1 ± 0.59	(8.7 ± 1.2)
	0.7	0.69 ± 0.01	(0.70 ± 0.01)	**10**	7.3 ± 0.58	(8.3 ± 1.3)
	0.8	0.78 ± 0.02	(0.80 ± 0.02)	**10**	5.4 ± 0.82	(7.0 ± 1.4)
	0.9	0.87 ± 0.02	(0.90 ± 0.02)	**10**	1.1 ± 0.94	(3.3 ± 2.0)
10	**0.1**	0.1 ± 0.01	(0.10 ± 0.01)	**10**	9.64 ± 0.51	(9.77 ± 1.1)
	0.2	0.2 ± 0.01	(0.20 ± 0.01)	**10**	9.02 ± 0.52	(9.47 ± 1.1)
	0.3	0.3 ± 0.01	(0.30 ± 0.01)	**10**	8.38 ± 0.55	(9.05 ± 1.2)
	0.4	0.4 ± 0.01	(0.40 ± 0.01)	**10**	7.6 ± 0.69	(8.62 ± 1.3)
	0.5	0.49 ± 0.01	(0.50 ± 0.01)	**10**	6.6 ± 0.61	(7.53 ± 1.2)
	0.6	0.59 ± 0.01	(0.60 ± 0.01)	**10**	5.17 ± 0.74	(6.36 ± 1.5)
	0.7	0.68 ± 0.01	(0.70 ± 0.02)	**10**	2.93 ± 1.13	(4.38 ± 1.6)
	0.8	0.77 ± 0.02	(0.81 ± 0.02)	**10**	−1.05 ± 1.4	(0.5 ± 2.4)
	0.9	0.86 ± 0.02	(0.91 ± 0.02)	**10**	−9.79 ± 2.84	(−12 ± 5.6)
3	**0.1**	0.1 ± 0.01	(0.1 ± 0.01)	**10**	8.57 ± 0.53	(9.02 ± 1.2)
	0.2	0.2 ± 0.01	(0.2 ± 0.01)	**10**	7.11 ± 0.74	(7.96 ± 1.2)
	0.3	0.3 ± 0.01	(0.3 ± 0.01)	**10**	5.37 ± 0.76	(6.62 ± 1.5)
	0.4	0.39 ± 0.01	(0.41 ± 0.01)	**10**	3.38 ± 1.09	(4.57 ± 1.8)
	0.5	0.49 ± 0.01	(0.51 ± 0.01)	**10**	0.4 ± 1.33	(2 ± 2.3)
	0.6	0.58 ± 0.01	(0.61 ± 0.01)	**10**	−3.31 ± 1.95	(−1.8 ± 2.5)
	0.7	0.67 ± 0.02	(0.71 ± 0.02)	**10**	−9.38 ± 2.69	(−9.2 ± 3.6)
	0.8	0.77 ± 0.02	(0.81 ± 0.02)	**10**	−20.91 ± 5.11	(−25 ± 7.1)
	0.9	0.86 ± 0.02	(0.92 ± 0.02)	**10**	−50.28 ± 13.55	(−121 ± 67)

The spectral densities have been simulated with Equation (5), for three different global correlation times ($\tau_c = 3$, 10 and 30 ns), a τ_f of 10 ps, and a generalized order parameter $0.1 < S^2 < 0.9$. S^2 and τ_f values used for the simulation are indicated in bold characters. Such parameters are characteristic of a slow tumbling protein, experiencing more or less restricted internal fast motions.

(7) is required. The "extended" formalism was also necessary to correctly describe the dynamics of the NH vectors located in the solvent-exposed Glu35-Leu40 peptidic segment and in the long flexible loop, including residues in the N-terminal turns of the helix (Arg56, Ser58, His59 and Leu60). The use of the "extended" model was fully justified by a significantly smaller χ^2, and reasonable values of τ_s (0.5–1.5 ns). On the other hand, the use of Equation (11) was needed for some residues, indicating the presence of motions in the μs–ms range. The results of the dynamics analysis of $p13^{MTCP1}$ are gathered on Figure 8: for the sake of clarity, only results from the classical spectral density mapping have been reported.

Figure 9 shows a comparison between the generalized order parameters S^2 and correlation times (τ_f, τ_s) obtained either from the "model-free" analysis of the spectral densities calculated with the conventional or the fast spectral density mapping. The two strategies yield very similar S^2 parameters regardless of the formalism which has been used, whereas some discrepancies appear on the correlation times values: if the two approaches give usually similar values for τ_s, τ_f values are generally slightly underestimated when

Table 2. Motion parameters obtained by fitting simulated spectral densities obtained either with the conventional spectral density mapping or with the fast spectral density mapping (into brackets) in the case of the Extended Lipari–Szabo model (τ_c was fixed at the value used in the simulations)

Extended Lipari–Szabo Model: Random Motion									
τ_c(ns)	S_s^2			S_f^2			τ_s(ps)		
30	**0.1**	0.13 ± 0.01	(0.12 ± 0.01)	**0.1**	0.08 ± 0.01	(0.08 ± 0.01)	**300**	423 ± 20	(496 ± 35)
	0.2	0.24 ± 0.02	(0.24 ± 0.02)	**0.2**	0.16 ± 0.01	(0.18 ± 0.01)	**300**	417 ± 25	(474 ± 33)
	0.3	0.36 ± 0.02	(0.36 ± 0.02)	**0.3**	0.25 ± 0.01	(0.27 ± 0.01)	**300**	424 ± 21	(472 ± 38)
	0.4	0.47 ± 0.02	(0.47 ± 0.02)	**0.4**	0.35 ± 0.01	(0.36 ± 0.01)	**300**	418 ± 24	(459 ± 39)
	0.5	0.57 ± 0.02	(0.58 ± 0.03)	**0.5**	0.45 ± 0.01	(0.46 ± 0.01)	**300**	419 ± 28	(452 ± 38)
	0.6	0.67 ± 0.02	(0.67 ± 0.02)	**0.6**	0.55 ± 0.02	(0.57 ± 0.02)	**300**	416 ± 36	(442 ± 43)
	0.7	0.76 ± 0.01	(0.76 ± 0.02)	**0.7**	0.66 ± 0.02	(0.67 ± 0.02)	**300**	417 ± 42	(433 ± 36)
	0.8	0.85 ± 0.01	(0.84 ± 0.02)	**0.8**	0.77 ± 0.03	(0.77 ± 0.03)	**300**	403 ± 53	(440 ± 53)
	0.9	0.93 ± 0.01	(0.92 ± 0.01)	**0.9**	0.9 ± 0.03	(0.88 ± 0.03)	**300**	366 ± 83	(451 ± 115)
10	**0.1**	0.13 ± 0.01	(0.14 ± 0.02)	**0.1**	0.08 ± 0.01	(0.08 ± 0.01)	**300**	423 ± 26	(478 ± 41)
	0.2	0.25 ± 0.02	(0.26 ± 0.02)	**0.2**	0.16 ± 0.01	(0.17 ± 0.01)	**300**	423 ± 29	(463 ± 42)
	0.3	0.36 ± 0.02	(0.37 ± 0.02)	**0.3**	0.25 ± 0.01	(0.26 ± 0.01)	**300**	423 ± 31	(452 ± 43)
	0.4	0.47 ± 0.02	(0.48 ± 0.03)	**0.4**	0.34 ± 0.01	(0.35 ± 0.01)	**300**	422 ± 41	(446 ± 49)
	0.5	0.58 ± 0.02	(0.58 ± 0.03)	**0.5**	0.44 ± 0.01	(0.45 ± 0.02)	**300**	416 ± 50	(428 ± 52)
	0.6	0.68 ± 0.02	(0.67 ± 0.03)	**0.6**	0.54 ± 0.02	(0.55 ± 0.02)	**300**	409 ± 60	(438 ± 68)
	0.7	0.78 ± 0.02	(0.76 ± 0.03)	**0.7**	0.65 ± 0.02	(0.65 ± 0.02)	**300**	391 ± 81	(433 ± 87)
	0.8	0.87 ± 0.01	(0.84 ± 0.03)	**0.8**	0.77 ± 0.02	(0.76 ± 0.03)	**300**	343 ± 88	(478 ± 129)
	0.9	0.93 ± 0.08	(0.92 ± 0.04)	**0.9**	0.91 ± 0.12	(0.89 ± 0.06)	**300**	246 ± 124	(453 ± 272)
3	**0.1**	0.13 ± 0.04	(0.21 ± 0.04)	**0.1**	0.08 ± 0.01	(0.08 ± 0.01)	**300**	430 ± 63	(377 ± 78)
	0.2	0.26 ± 0.03	(0.31 ± 0.05)	**0.2**	0.16 ± 0.01	(0.17 ± 0.03)	**300**	418 ± 62	(383 ± 108)
	0.3	0.38 ± 0.04	(0.42 ± 0.07)	**0.3**	0.25 ± 0.01	(0.27 ± 0.07)	**300**	412 ± 89	(349 ± 141)
	0.4	0.5 ± 0.03	(0.49 ± 0.1)	**0.4**	0.34 ± 0.01	(0.4 ± 0.16)	**300**	399 ± 98	(337 ± 166)
	0.5	0.62 ± 0.03	(0.54 ± 0.13)	**0.5**	0.43 ± 0.02	(0.56 ± 0.23)	**300**	349 ± 101	(335 ± 225)
	0.6	0.72 ± 0.02	(0.62 ± 0.12)	**0.6**	0.53 ± 0.02	(0.66 ± 0.21)	**300**	333 ± 101	(387 ± 276)
	0.7	0.79 ± 0.11	(0.7 ± 0.12)	**0.7**	0.69 ± 0.20	(0.75 ± 0.19)	**300**	260 ± 133	(417 ± 347)
	0.8	0.74 ± 0.21	(0.78 ± 0.11)	**0.8**	0.81 ± 0.11	(0.86 ± 0.14)	**300**	178 ± 227	(661 ± 1217)
	0.9	– ± –	(– ± –)	**0.9**	– ± –	(0.86 ± 0.06)	**300**	– ± –	(– ± –)

The spectral densities have been simulated with Equation (7) for three different global correlation times ($\tau_c = 3$, 10 and 30 ns), a τ_s of 300 ps, and partial order parameter $0.1 < S_f^2 = S_s^2 < 0.9$. S_f^2, S_s^2 and τ_f values used for the simulation are indicated in bold characters. Such parameters are characteristic of a more or less disordered peptidic segment in a slow tumbling protein.

using the fast spectral density mapping, even if they remain of the same order of magnitude. Moreover, exchange contributions deduced from the two strategies are of comparable magnitude and concern the same residues (Figure 10). These values are also comparable to the ones obtained by following the approach proposed by Habazettl et al. (1995), where the ϕ values are deduced from the linear dependence of $2R_2 - R_1$ with the square of the Larmor frequencies ω_N^2. As usually observed when using this latter approach in cojunction with Lipari–Szabo formalisms, significant exchange contributions are detected for almost all backbone NH bonds. This suggests the presence of widespread exchange processes for $p13^{MTCP1}$. However, numerous small ϕ values could either be indicative of an unidentified global exchange process, for example due to protein aggregation, or reflect an artifact arising from the Lipari–Szabo formalism when using a single τ_c. It has been shown for another protein (Bouguet-Bonnet et al., 1995a, b) that the use of an effective τ_c for each residue considerably reduces the number of NH bonds exhibiting small ϕ values. Nevertheless, significant increases in ϕ values (up to 3×10^{-17} s/rad) are observed for residues which need the use

Table 3. Motion parameters obtained by fitting simulated spectral densities obtained either with the conventional spectral density mapping or with the fast spectral density mapping (into brackets) in the case of the Extended Lipari–Szabo model (τ_c was fixed at the value used in the simulations)

Extended Lipari–Szabo Model: Hinge Motion									
τ_c(ns)	S_s^2			S_f^2			τ_s (ps)		
30	**0.8**	0.85 ± 0.01	(0.84 ± 0.02)	**0.1**	0.1 ± 0.01	(0.1 ± 0.01)	**300**	411 ± 50	(438 ± 53)
	0.8	0.85 ± 0.01	(0.84 ± 0.02)	**0.2**	0.19 ± 0.01	(0.19 ± 0.01)	**300**	411 ± 57	(432 ± 52)
	0.8	0.85 ± 0.01	(0.84 ± 0.02)	**0.3**	0.29 ± 0.01	(0.29 ± 0.01)	**300**	406 ± 50	(427 ± 53)
	0.8	0.85 ± 0.01	(0.84 ± 0.02)	**0.4**	0.39 ± 0.01	(0.39 ± 0.01)	**300**	401 ± 54	(437 ± 61)
	0.8	0.85 ± 0.01	(0.84 ± 0.02)	**0.5**	0.48 ± 0.02	(0.48 ± 0.01)	**300**	401 ± 55	(439 ± 51)
	0.8	0.85 ± 0.01	(0.84 ± 0.02)	**0.6**	0.57 ± 0.02	(0.58 ± 0.02)	**300**	421 ± 54	(442 ± 54)
	0.8	0.85 ± 0.01	(0.84 ± 0.02)	**0.7**	0.68 ± 0.03	(0.67 ± 0.02)	**300**	403 ± 48	(452 ± 59)
	0.8	0.85 ± 0.01	(0.84 ± 0.02)	**0.8**	0.77 ± 0.02	(0.77 ± 0.03)	**300**	408 ± 53	(438 ± 60)
	0.8	0.85 ± 0.01	(0.84 ± 0.02)	**0.9**	0.87 ± 0.03	(0.87 ± 0.03)	**300**	402 ± 61	(435 ± 55)
10	**0.8**	0.86 ± 0.01	(0.84 ± 0.04)	**0.1**	0.1 ± 0.01	(0.1 ± 0.01)	**300**	370 ± 96	(451 ± 156)
	0.8	0.86 ± 0.01	(0.85 ± 0.04)	**0.2**	0.19 ± 0.01	(0.19 ± 0.01)	**300**	369 ± 105	(459 ± 139)
	0.8	0.86 ± 0.01	(0.85 ± 0.03)	**0.3**	0.29 ± 0.01	(0.29 ± 0.02)	**300**	358 ± 98	(442 ± 147)
	0.8	0.86 ± 0.01	(0.85 ± 0.03)	**0.4**	0.38 ± 0.01	(0.38 ± 0.02)	**300**	348 ± 90	(463 ± 154)
	0.8	0.86 ± 0.01	(0.84 ± 0.04)	**0.5**	0.48 ± 0.01	(0.48 ± 0.03)	**300**	364 ± 96	(448 ± 147)
	0.8	0.86 ± 0.01	(0.84 ± 0.05)	**0.6**	0.57 ± 0.01	(0.58 ± 0.05)	**300**	346 ± 88	(443 ± 146)
	0.8	0.87 ± 0.01	(0.84 ± 0.03)	**0.7**	0.67 ± 0.02	(0.67 ± 0.03)	**300**	342 ± 98	(451 ± 145)
	0.8	0.86 ± 0.01	(0.85 ± 0.04)	**0.8**	0.76 ± 0.02	(0.77 ± 0.06)	**300**	367 ± 103	(446 ± 143)
	0.8	0.87 ± 0.01	(0.85 ± 0.03)	**0.9**	0.86 ± 0.02	(0.86 ± 0.04)	**300**	353 ± 77	(453 ± 142)
3	**0.8**	0.72 ± 0.22	(0.79 ± 0.10)	**0.1**	0.13 ± 0.05	(0.1 ± 0.02)	**300**	188 ± 273	(611 ± 723)
	0.8	0.74 ± 0.2	(0.80 ± 0.09)	**0.2**	0.25 ± 0.08	(0.21 ± 0.03)	**300**	157 ± 225	(526 ± 588)
	0.8	0.75 ± 0.21	(0.75 ± 0.13)	**0.3**	0.37 ± 0.13	(0.33 ± 0.06)	**300**	198 ± 295	(626 ± 1805)
	0.8	0.77 ± 0.21	(0.80 ± 0.11)	**0.4**	0.48 ± 0.19	(0.41 ± 0.07)	**300**	225 ± 293	(570 ± 665)
	0.8	0.76 ± 0.21	(0.79 ± 0.11)	**0.5**	0.61 ± 0.24	(0.53 ± 0.08)	**300**	184 ± 223	(580 ± 942)
	0.8	0.73 ± 0.21	(0.78 ± 0.15)	**0.6**	0.77 ± 0.29	(0.63 ± 0.01)	**300**	191 ± 297	(698 ± 1494)
	0.8	0.75 ± 0.2	(0.77 ± 0.10)	**0.7**	0.85 ± 0.31	(0.75 ± 0.14)	**300**	180 ± 202	(576 ± 635)
	0.8	0.76 ± 0.2	(0.78 ± 0.11)	**0.8**	0.96 ± 0.32	(0.87 ± 0.16)	**300**	175 ± 174	(501 ± 683)
	0.8	0.72 ± 0.22	(0.80 ± 0.09)	**0.9**	– ± –	(0.93 ± 0.14)	**300**	191 ± 442	(630 ± 704)

The spectral densities have been simulated with Equation (7) for three different global correlation times ($\tau_c = 3$, 10 and 30 ns), a τ_s of 300 ps, and partial order parameter $S_f^2 = 0.8$ and $0.1 < S_s^2 < 0.9$. S_f^2, S_s^2, τ_c and τ_f values used for the simulation are reported in bold characters. Such parameters are characteristic of a peptidic segment experiencing more or less restricted collective hinge motions in a slow tumbling protein.

of Equation (11): this provides some confidence concerning the Lipari–Szabo formalisms (simple or extended, regardless of the strategy used (SDM or FSDM) for obtaining the spectral densities.

Concluding remarks

The analysis of relaxation data obtained at n fields using the approach described above results in the production of $n + 2$ points for the discrete sampling of the spectral density function ($J(0)$, $nJ(\omega_N)$ and $\langle J(\omega_H)\rangle$), through the measurement of $n + 2$ relaxation experiments: nR_1 rate constants (at each NMR field), one R_2 rate constant and one NOE measurement at a single NMR field. This yields a considerable saving of measurement time when compared to the conventional spectral density mapping approach, where $3n$ relaxation measurements are needed to obtain $2n + 1$ discrete points on the spectral density curve, hence the name of ''fast spectral density mapping''. Thus, the dynamics analysis of the protein p13^{MTCP1}

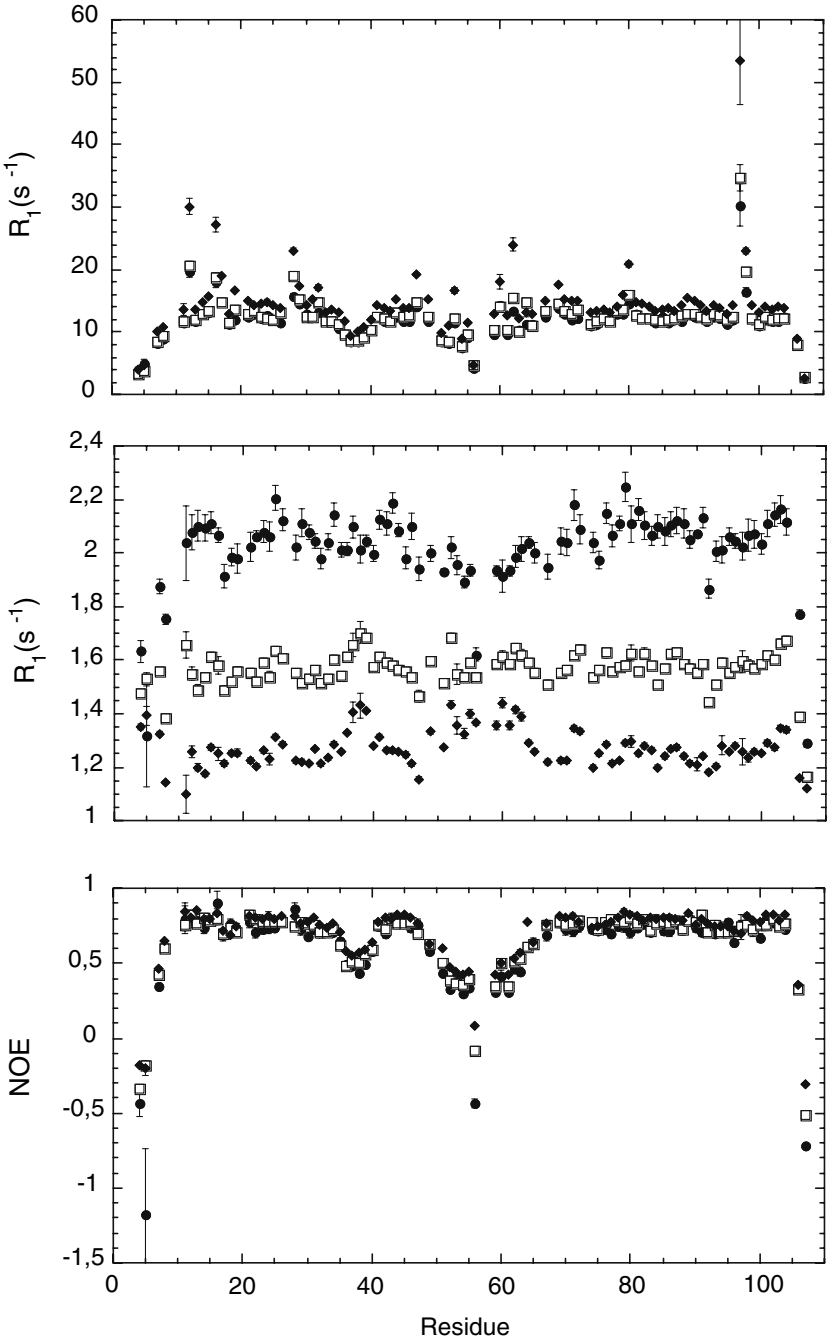

Figure 6. Relaxation rates constants and $^{15}N\{^{1}H\}$NOEs, as a function of the p13^{MTCP1} sequence, measured for at 9.4 T (filled circles), 11.75 T (open squares) and 14.1 T (filled diamonds). The relaxation rate constants R_1 and the R_2 were obtained from non-linear fits of peak heights (Skelton et al., 1993) to monoexponential functions (Press et al., 1986). The uncertainties were determined from 500 data sets generated according to the Monte Carlo procedure. The $^{15}N\{^{1}H\}$NOE is deduced from the ratio of peak heights obtained with and without proton saturation.

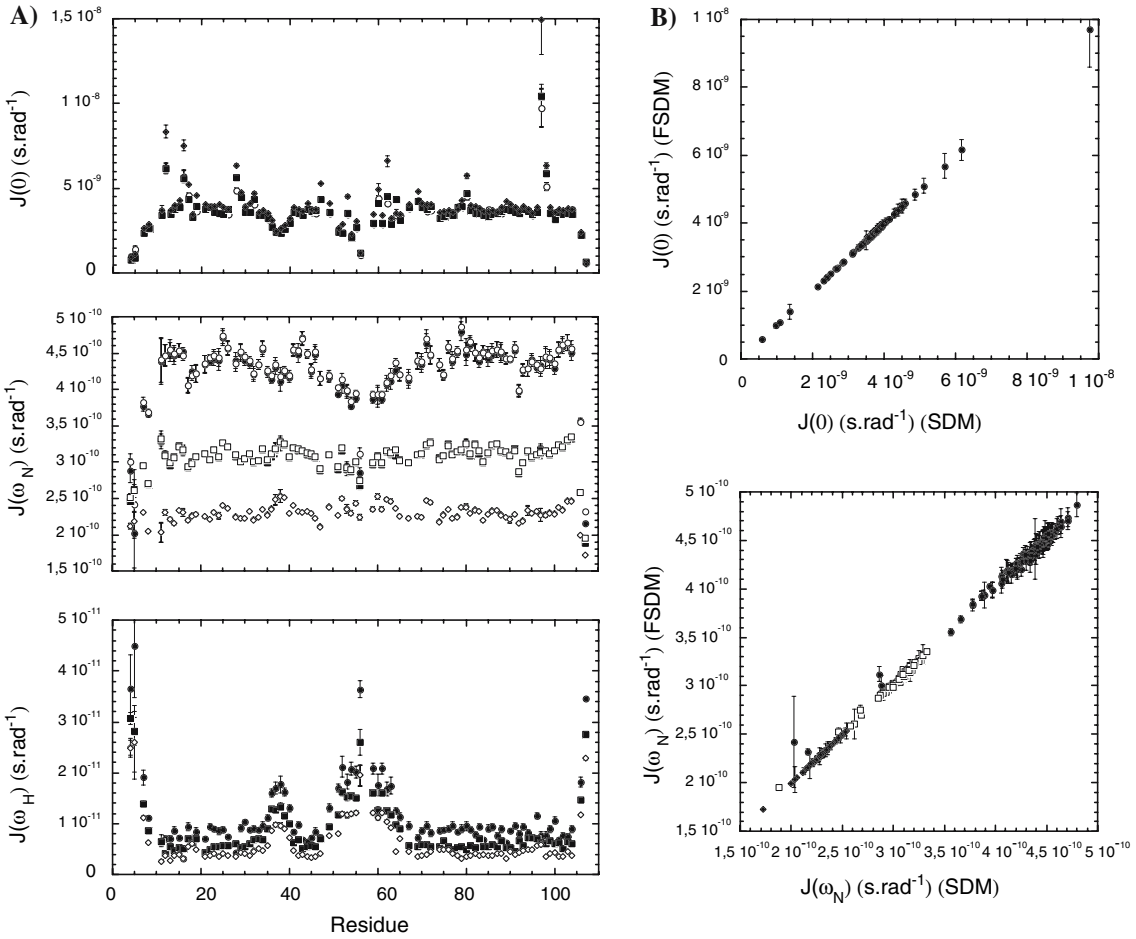

Figure 7. (A) Spectral density functions, as a function of the p13^{MTCP1} sequence, obtained from relaxation rates measured at 9.4 T (circles), 11.75 T (squares) and 14.1 T (diamonds): filled symbols corresponds to spectral densities calculated using the conventional spectral density mapping, open symbols to spectral densities calculated using the fast spectral density mapping. (B) Comparison of $J(0)$ (top) and $J(\omega_N)$ (bottom) values obtained for p13^{MTCP1} with either the regular or the fast spectral density mapping. For the sake of clarity and concerning $J(0)$ values calculated with the regular spectral density mapping method, only the ones deduced from relaxation parameters measured at 9.4 T are reported. Filled circles, open squares and filled diamonds stand for $J(40)$, $J(50)$ and $J(60)$, respectively.

through the conventional spectral density mapping at three NMR field strengths needs about seven days of spectrometer measuring time, whereas omitting the measurement of R_2 relaxation rates at 11.75 and 14.1 T as well as the $^{15}N\{^1H\}$NOEs at 9.4 T and 11.75 T reduces this measuring time to less than 4 days. Note that the time saving which arises from this strategy will continue to increase with the number of different NMR fields used for the measurement of the ^{15}N heteronuclear relaxation parameters!

The choice of the NMR fields in the simulations and the practical example presented above is not arbitrary : measuring R_2 at the lower magnetic field strength should minimize possible exchange contributions, and prevent some experimental artifacts such as offset effects due to the ^{15}N radio-frequency pulse lengths in the CPMG sequence. Contrary to CPMG experiments, experimental schemes designed for R_1 measurements are relatively insensitive to experimental artifacts as well as to variations of the probe performances from a spectrometer to another (RF heating,...), so that one can expect reliable measurements at any fields. On the other hand, due to the relatively low sensitivity of NOE experiments, this parameter should be

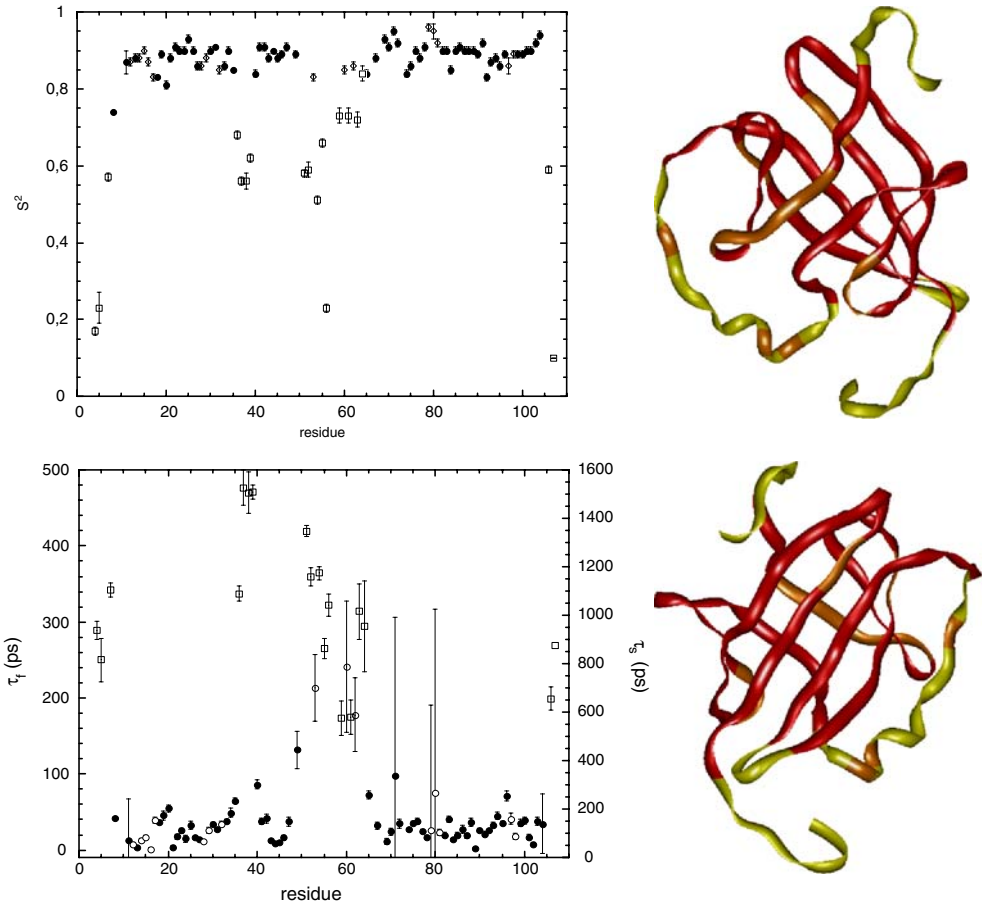

Figure 8. (Left) Dynamical parameters obtained for p13^{MTCP1} through the analysis of the spectral densities – calculated with the conventional spectral density mapping approach – with the program DYNAMOF: generalized order parameters S^2 (top) and correlation times τ_f and τ_s (bottom) are plotted versus the residue number in the protein sequence. The use of the different symbols indicate the use of the "simple" Lipari–Szabo formalism (filled circles) (Equation (5)), with possible additional exchange contributions (open circles) (Equation (11)), or of the "extended" Lipari–Szabo formalism (open squares) (Equation (7)). The uncertainties were determined from 500 data sets generated according to the Monte Carlo procedure. (Right) Two views – related by a 180° rotation around the vertical axis – of the ribbon representation of p13^{MTCP1}: the color code indicates the use of Equation (5) (red), (7) (yellow) or (11) (orange) for the best fit of the spectral density function of the corresponding residue.

better measured at the highest available NMR field. Note that other combinations are possible: among others, one can choose to use the same field for measuring R_2 and NOE. This yields two "exact" values for both $J(0)$ and ($\langle J(\omega_H)\rangle$, instead of only one $\langle J(\omega_H)\rangle$ with the previous combination. Nevertheless, due to the extremely weak deviations reported for the $J(0)$ values simulated with "wrong" values of σ_{NH} (Figure 1), the determination of its "exact" value is of little practical interest.

In the present calculations, we assume a constant value for the ^{15}N chemical shift anisotropy (CSA) over the whole protein sequence although site-specific variations in both the magnitude and orientation the ^{15}N CSA tensor has been pointed out (Fushman et al., 1998). Thus, when using dedicated relaxation experiments and strategies (for a review: Fushman and Cowburn, 2001), ^{15}N $\Delta\sigma$ values observed in ubiquitine range from −116 to −231 ppm. It is, however, difficult to find a strong correlation between the "experimental" value of this parameter and the nature of the relevant residue or the possible involvement of this residue in a structured area of the protein. More recently, the ^{15}N CSA have been measured in ubiquitine dissolved in a dilute liquid crystal-

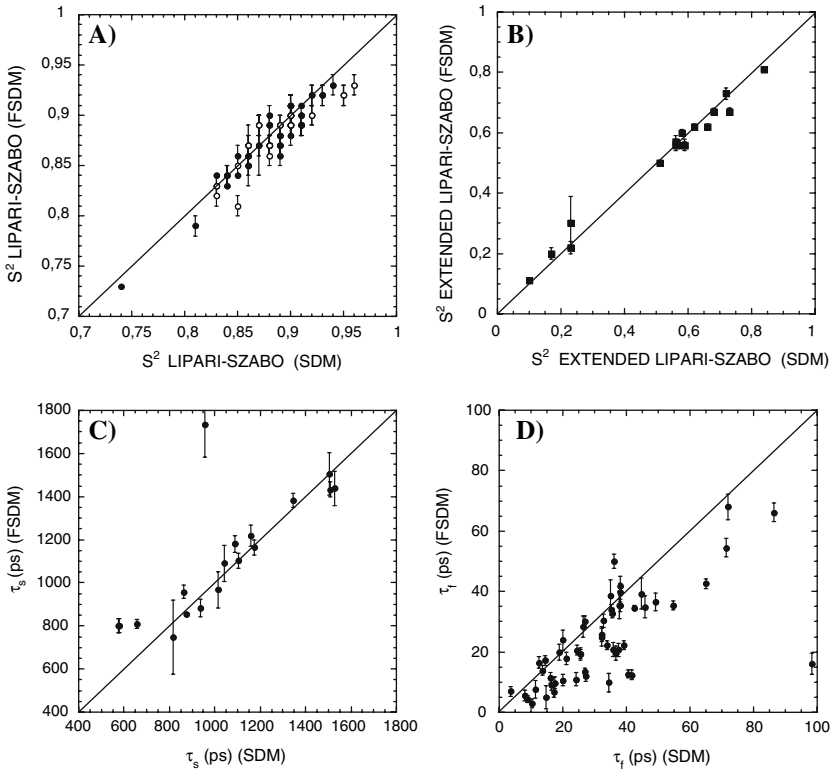

Figure 9. Comparison of the dynamical parameters obtained for p13^{MTCP1} through the "model-free" analysis of the spectral densities calculated either with the conventional or the fast spectral density mapping. (A) and (B): S^2 and τ_f obtained with the "simple" Lipari–Szabo model (filled circles) (Equation (5)), with possible contributions from exchange process (open circles) (Equation (11)). (C) and (D): S^2 ($S_f^2 S_s^2$) and τ_s obtained with the "extended" Lipari–Szabo model (Equation (7)).

line phase: the tensor values have been derived from the change in chemical shift between the oriented and isotropic states (Cornilescu and Bax, 2000). These experiments show little variation in the magnitude of $\Delta\sigma$, but significant variations in the tensor rhombicity that anyway have a small effect on the auto-relaxation rates. Finally, using measurements carried out at five magnetic fields on another small protein (p8^{MTCP1}), we were unable to found CSA variations greater than the "statistical uncertainties" (Canet et al., 2001; Bouguet-Bonnet et al., 2005a, b). Nevertheless, even if this question is still strongly debated, we must borne in mind that ignoring a possible variation of the ^{15}N CSA will result in (limited) errors in $J(0)$ as – to a lesser extent – in ($J\omega_N$) values, which in turn could yield erroneously R_{ex} terms, since they have the same field dependence as the CSA contribution to R_2. In the case of p13^{MTCP1}, R_{ex} contributions to $J(0)$ are detected for the same residues whatever the strategy used ("Conventional" or Fast Spectral Density Mapping, or field dependance of $2R_2 - R_1$), even if differences in magnitude are noticeable, depending on the chosen method. The fact that these contributions concern residues involved in "excited-states" of the protein (Mulder et al., 2001), as it has been shown previously by high-pressure NMR experiments performed on p13^{MTCP1} (Kitahara et al., 2002) strongly supports the reliability of these results. The differences on the R_{ex} magnitude can be explained by the fact that none of the methods used here is really suitable for an accurate quantification of these contributions which would need specifically designed experiments such as relaxation dispersion experiments (Mulder et al., 2001; Tollinger et al., 2001).

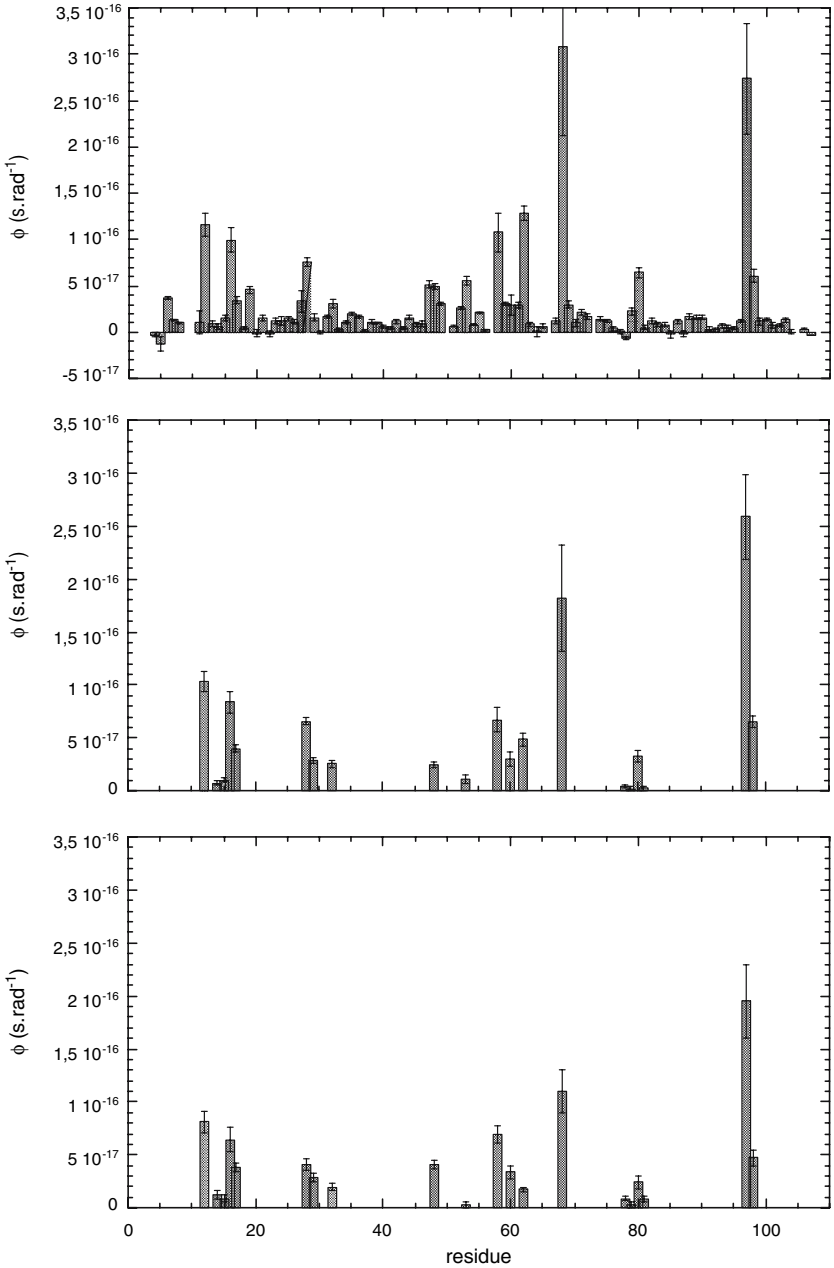

Figure 10. Plot of the exchange factor ϕ versus the residue number in the p13^{MTCP1} sequence of. The ϕ values were obtained from the linear dependence of $2R_2$-R_1 with the square of the Larmor frequency ω_N^2 (top); directly from the fit of the spectral densities obtained with the conventional (middle) or the fast (bottom) spectral density mapping approach with Equation (11).

Acknowledgments

The authors are grateful to the "Association pour la Recherche sur le Cancer" for a research grant. V. Ropars is supported by the "Ligue Nationale contre le Cancer".

References

Abragam, A. (1961) *Principles of Nuclear Magnetism*, Oxford Science Publication, Clarendon Press, Oxford.

Atkinson, R.A. and Kieffer, B. (2004) *Progress in Nuclear Magnetic Resonance Spectroscopy*, **44**, 141–187.

Austin, R.H., Beeson, K.W., Eisenstein, L., Frauenfelder, H. and Gunsalus, I.C. (1975) *Biochemistry*, **14**, 5355–5373.

Barthe, P., Chiche, L., Declerck, N., Delsuc, M.-A., Lefèvre, J.-F., Malliavin, T., Mispelter, J., Stern, M.-H., Lhoste, J.M. and Roumestand, C. (1999) *J. Biomol. NMR*, **15**, 271–288.

Barthe, P., Ropars, V. and Roumestand, C. (2006) *C. R. Chimie* **9**, 503–513.

Bouguet-Bonnet, S., Mutzenhardt, P., Roumestand, C. and Canet, D. (2005a) *Concepts in Magnetic Resonance*, **24**(1), 1–9.

Bouguet-Bonnet, S., Mutzenhardt, P., Roumestand, C. and Canet, D. (2005b) *Concepts in Magnetic Resonance*, **24**(1), 10–16.

Canet, D., Barthe, P., Mutzenhardt, P. and Roumestand, C. (2001) *J. Am. Chem. Soc.*, **123**(19), 4567–4576.

Carr, H.Y. and Purcell, E.M. (1954) *Phys. Rev.*, **94**, 630–632.

Clore, G.M., Szabo, A., Bax, A., Kay, L.E., Driscoll, P.C., Wingfield, P.T. and Gronenborn, A.M. (1990a) *J. Am. Chem. Soc.*, **112**, 4989–4991.

Clore, G.M., Driscoll, P.C., Wingfield, P.T. and Gronenborn, A.M. (1990b) *Biochemistry*, **29**, 7387–7401.

Cornilescu, G. and Bax, A. (2000) *J. Am. Chem. Soc.*, **122**, 10143–10154.

Eisenmesser, E.Z., Millet, O., Labeikovsky, W., Korzhnev, D.M., Wolf-Watz, M., Bosco, D.A., Skalicky, J.J, Kay, L.E. and Kern, D. (2005) *Nature*, **438**, 117–121.

Farrow, N.A., Zhang, O., Szabo, A., Torchia, D.A. and Kay, L.E. (1995) *J. Biomol. NMR*, **6**, 153–162.

Fushman, D., Tjandra, N. and Cowburn, D. (1998) *J. Am. Chem. Soc.*, **120**, 10947–10952.

Fushman, D., Tjandra, N. and Cowburn, D. (1999) *J. Am. Chem. Soc.*, **121**, 8577–8582.

Fushman, D. and Cowburn, D. (2001) *Methods Enzymol.*, **339**, 109–126.

Guignard, L., Padilla, A., Mispelter, J., Yang, Y.-S., Stern, M.-H., Lhoste, J.M. and Roumestand, C. (2000) *J. Biomol. NMR*, **17**, 215–230.

Habazettl, J. and Wagner, G. (1995) *J. Magn. Reson.*, **B109**, 100–104.

Ishima, R. and Nagayama, K. (1995a) *Biochemistry*, **34**, 3162–3171.

Ishima, R. and Nagayama, K. (1995b) *J. Magn. Reson.*, **B108**, 73–76.

Kay, L.E., Torchia, D.A. and Bax, A. (1989) *Biochemistry*, **28**, 8972–8979.

Kay, L.E., Nicholson, L.K., Delaglio, F., Bax, A. and Torchia, D.A. (1992) *J. Magn. Reson.*, **97**, 359–375.

Kitahara, R., Royer, C., Yamada, H., Boyer, M., Saldana, J.-L., Akasaka, K. and Roumestand, C. (2002) *J. Mol Biol.*, **320**, 609–628.

Lefèvre, J.-F., Dayie, K.T., Peng, J.W. and Wagner, G. (1996) *Biochemistry*, **35**, 2674–2686.

Lienin, S.F., Bremi, T., Brutscher, B., Brushweiler, R. and Ernst, R.R. (1998) *J. Am. Chem. Soc.*, **120**, 9870–9879.

Lipari, G. and Szabo, A. (1982) *J. Am. Chem. Soc.*, **104**, 4546–4559.

Marion, D., Ikura, M., Tschudin, R. and Bax, A. (1989b) *J. Magn. Reson.*, **85**, 393–399.

Meiboom, S. and Gill, D. (1958) *Rev. Sci. Instrum.*, **29**, 688–691.

Mulder, F.A.A., Mittermaier, A., Hon, B., Dahlquist, F.W. and Kay, L.E. (2001) *Nature Struct. Biol.*, **8**, 932–935.

Palmer, A.G. (2004) *Chem. Rev.*, **104**, 3623–3640.

Peng, J.W. and Wagner, G. (1992a) *Biochemistry*, **31**, 8571–8586.

Peng, J.W. and Wagner, G. (1992b) *J. Magn. Reson.*, **98**, 308–332.

Peng, J.W. and Wagner, G. (1995) *Biochemistry*, **34**, 16733–16752.

Piotto, M., Saudek, V. and Sklenar, V. (1992) *J. Biomol. NMR*, **2**, 661–665.

Press, W.H., Flannery, B.P., Teukolsky, S.A. and Vetterling, W.T. (1986) *Numerical Recipes*, Cambridge University Press, Cambridge.

Skelton, N.J., Palmer, A.G. III, Akke, M., Kördel, J., Rance, M. and Chazin, W.J. (1993) *J. Magn. Reson.*, **B102**, 253–264.

Sklenar, V. (1995) *J. Magn. Reson.*, **A114**, 132–135.

Tjandra, N., Feller, S.E., Pastor, R.W. and Bax, A. (1995) *J. Am. Chem. Soc.*, **117**, 12562–12566.

Tjandra, N., Szabo, A. and Bax, A. (1996) *J. Am. Chem. Soc.*, **118**, 6986–6991.

Tollinger, M., Skrynnikov, N.R., Mulder, F.A.A., Forman-Kay, J.D. and Kay, L.E. (2001) *J. Am. Chem. Soc.*, **123**, 11341–11352.

Vis, H., Vorgias, C.E., Wison, K.S., Kaptein, R. and Boelens, R. (1998) *J. Biomol. NMR*, **11**, 265–277.

Wagner, G. and Wüthrich, K. (1978) *Nature*, **275**, 247–248.

Yang, Y.-S., Guignard, L., Padilla, A., Hoh, F., Strub, M.P., Stern, M.-H., Lhoste, J.M. and Roumestand, C (1998) *J. Biomol. NMR*, **11**(3), 337–354.